Article

Copper Incorporated Molybdenum Trioxide Nanosheet Realizing High-Efficient Performance for Hydrogen Production

Pengzuo Chen *, Weixia Huang, Kaixun Li, Dongmei Feng and Yun Tong *

Department of Chemistry, Key Laboratory of Surface & Interface Science of Polymer Materials of Zhejiang Province, Zhejiang Sci-Tech University, Hangzhou 310018, China
* Correspondence: pzchen0421@126.com (P.C.); tongyun@mail.ustc.edu.cn (Y.T.)

Abstract: The development of highly active non-precious metal electrocatalysts is crucial for advancing the practical application of hydrogen evolution reaction (HER). Doping engineering is one of the important strategies to optimize the electrocatalytic activity of electrocatalysts. Herein, we put forward a simple strategy to optimize the catalytic activity of MoO_3 material by incorporating the Cu atoms into the interlayer (denoted as $Cu-MoO_3$). The prepared $Cu-MoO_3$ nanosheet has a larger surface area, higher conductivity, and strong electron interactions, which contributes to optimal reaction kinetics of the HER process. As a result, the $Cu-MoO_3$ nanosheet only needs a small overpotential of 106 mV to reach the geometric current density of 10 mA cm^{-2}. In addition, it also delivers a low Tafel slope of 83 mV dec^{-1}, as well as high stability and Faraday efficiency. Notably, when using the $Cu-MoO_3$ as a cathode to construct the water electrolyzer, it only needs 1.55 V to reach the 10 mA cm^{-2}, indicating its promising application in hydrogen generation. This work provides a novel type of design strategy for a highly active electrocatalyst for an energy conversion system.

Keywords: MoO_3 nanosheet; Cu doping; electronic regulation; hydrogen production; water electrolyzer

1. Introduction

The continuous use of fossil fuels leads to serious environmental pollution and energy crises, forcing people to seek a new type of energy system. Hydrogen, as an environmentally friendly and energy-dense fuel, is considered one of the best candidates to replace fossil fuels [1–3]. High-purity hydrogen can be prepared by electrocatalytic water-splitting technology, which is an important way to promote the large-scale production of hydrogen [4–7]. However, the slow kinetic process leads to low catalytic efficiency of both hydrogen evolution reaction (HER) and oxygen evolution reaction (OER), resulting in high cost [8–11]. The application of catalysts can effectively improve the HER efficiency, but currently, the best materials are still concentrated in noble metal systems [12–14]. The high cost and low reserve greatly limit the wide application of precious metal materials. Therefore, it is very important to develop non-precious metal electrocatalysts that can replace noble metals for hydrogen production.

In this regard, molybdenum oxide (MoO_3) is widely used for electrocatalysis because of its high activity, environmental friendliness, low cost, and high durability [15–17]. However, the simple MoO_3 has certain disadvantages as an HER electrocatalyst due to the strong Mo-H bond during the HER process, which largely limits the H_{ads} desorption step and hinders the reaction kinetics of hydrogen production [18,19]. Thus, the development of new regulation strategies to optimize the adsorption-free energy of Mo metal sites for hydrogen reaction intermediates is the key to improving the catalytic activity of MoO_3 material. Recently, a series of surface-interface chemical regulation strategies have been widely used to design novel electrode materials, including interface structure design, defect engineering, and metal cation or anion doping [20–25]. Among them, doping engineering is one of the more effective and commonly used methods. For example, the doping

of electron-rich dopants into the structure of MoO_3 can decrease the density of states, thereby weakening the Mo-H bonding during the HER process [26,27]. In addition, metal cation doping can introduce heterogeneous metal atoms as synergistic catalytic centers to accelerate the kinetics of HER catalytic reaction based on optimizing the electronic structure of MoO_3 material [28,29]. Although doping engineering exhibits significant advantages, there are no reports on improving the catalytic activity of MoO_3 by introducing atomic doping.

Herein, a controllable Cu atom-doped MoO_3 nanosheet is successfully designed by hydrothermal reaction and the disproportionation of Cu^+ under reflux conditions. The incorporation of Cu atoms into the MoO_3 interlayer can improve the surface area and conductivity of MoO_3 material, resulting in a faster electron transfer process as well as more catalytic active centers for HER. Benefiting from those advantages, the prepared Cu-MoO_3 nanosheet exhibits superior catalytic performance for HER in an alkaline medium. In addition, the constructed Cu-MoO_3//FeOOH-NF electrolyzer also displays a low voltage of 1.55 V at a current density of 10 mA cm^{-2}, along with high stability. This work provides a feasible idea for the design of novel and efficient non-precious metal electrocatalysts.

2. Results and Discussion

In this work, the Cu-doped MoO_3 nanosheet is synthesized by a two-step process. The MoO_3 nanosheet is firstly prepared by hydrothermal reaction, followed by the disproportionation of Cu^+ under reflux conditions. The powder X-ray diffraction (XRD) pattern is measured to analyze the phase of the Cu-doped MoO_3 nanosheet. As shown in Figure 1a, the XRD pattern of Cu-MoO_3 exhibits typical diffraction peaks, which can be ascribed to the phase of the MoO_3 sample. These diffraction peaks are consistent with the pure MoO_3 nanosheet, as shown in Figure S1. No diffraction peaks are observed for Cu-based nanoparticles, indicating the successfully doping of Cu atoms into the framework of the MoO_3 nanosheet. This strategy is likely to be the intercalation of copper atoms into the layers of MoO_3, benefiting from the layered structure of MoO_3 (Figure 1b).
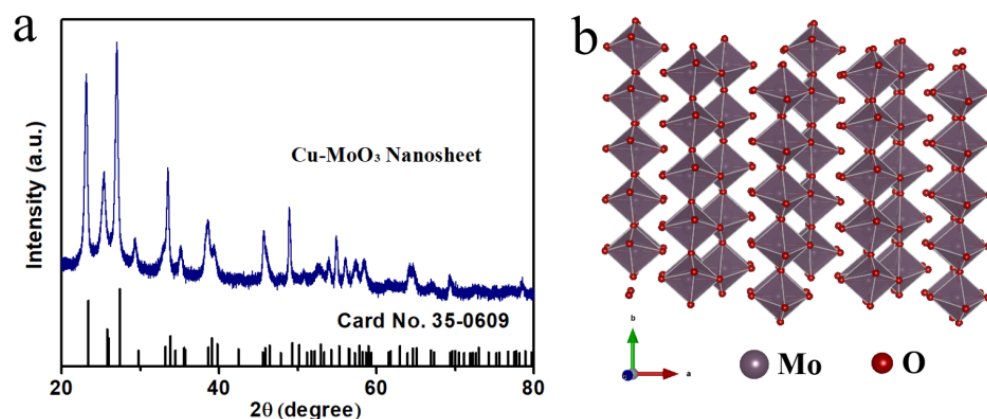

Figure 1. (**a**) The XRD pattern of Cu doped MoO_3 nanosheet and (**b**) the crystal structure of MoO_3 sample.

Transmission electron microscopy (TEM) is utilized to study the morphology of as-obtained products. As shown in Figure S2, the TEM images of pristine MoO_3 display the typical nanosheet morphology with a diameter of several hundred nanometers to micrometers. After the introduction of Cu atoms, the morphology of the nanosheet maintains well (Figure 2a–c). This result indicates that Cu doping does not cause significant changes in morphology. In addition, the high-resolution TEM (HRTEM) image is collected to study the microstructure of the Cu-MoO_3 nanosheet. In Figure 2d, the lattice fringe of 0.375 nm is consistent with the (110) plane of MoO_3. Furthermore, the energy dispersive X-ray spectroscopy elemental mapping images confirm the composition information of the Cu-MoO_3 nanosheet. As shown in Figure 3, the elements of Cu, Mo, and O are uniformly distributed

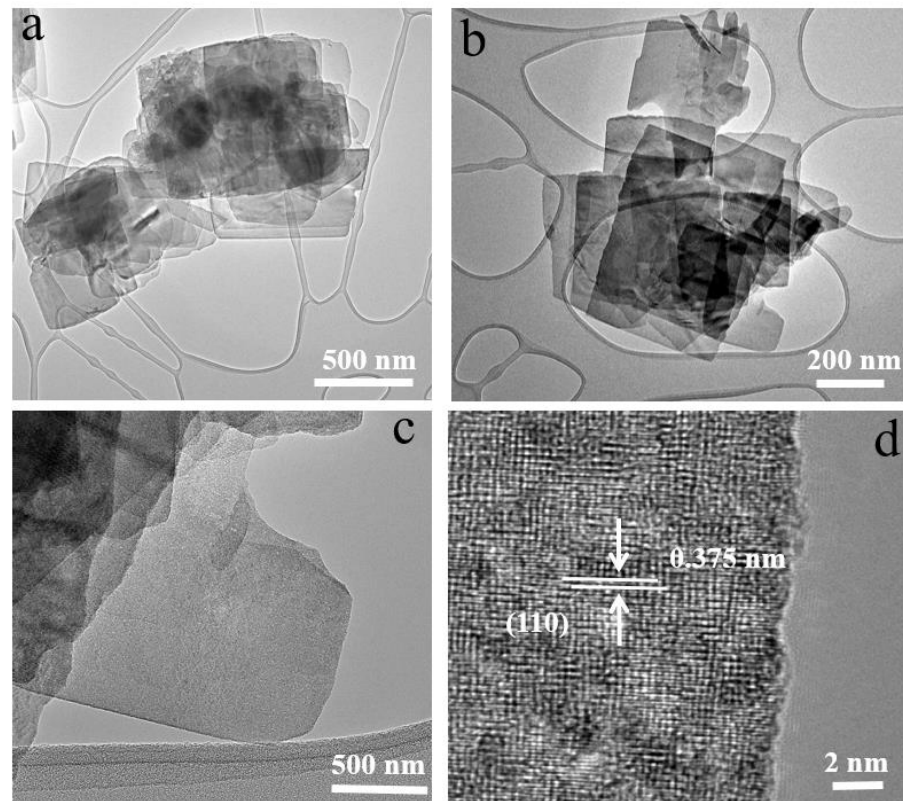throughout the whole MoO$_3$ nanosheet, indicating the successful doping of Cu atoms into the final samples.

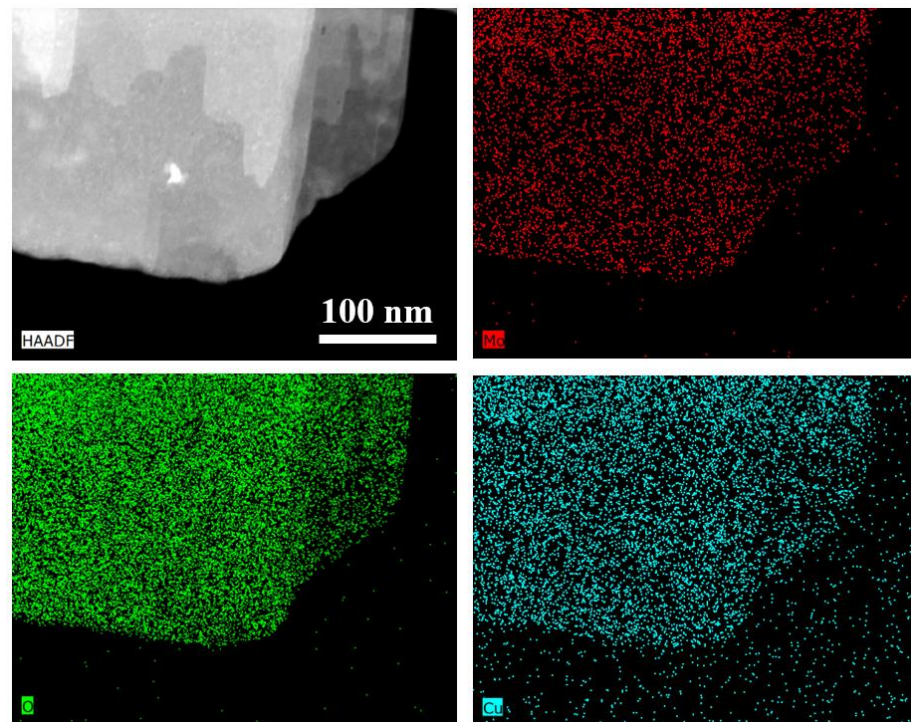**Figure 2.** (**a–c**) The TEM images and (**d**) HRTEM image of Cu doped MoO$_3$ nanosheet.

Figure 3. The elemental mapping images of Cu doped MoO$_3$ nanosheet.

The compositions and valence states of each element in the Cu-MoO$_3$ nanosheet are demonstrated by X-ray photoelectron spectroscopy (XPS). As shown in Figure 4a, the XPS survey of the Cu-MoO$_3$ nanosheet proves the composition of Mo (23.3%), Cu (8.4%) and O (68.3%) elements, which are consistent with the above elemental mapping images. In a contrast, the XPS survey of pristine MoO$_3$ nanosheet shows the contents of Mo and O elements without Cu signal (Figure S3). In addition, the high-resolution Mo 3d spectrum is shown in Figure 4b. The peaks located at the binding energy of 233.4 eV and 236.5 eV can be attributed to the Mo 3d 2p$_{5/2}$ and Mo 2p$_{3/2}$, which is the characteristic peaks of Mo^{6+} [26]. In addition, the two peaks located at the binding energy of 232.8 eV and 235.9 eV belong to the characteristic peaks of Mo^{4+} 2p$_{5/2}$ and Mo^{4+} 2p$_{3/2}$ [18]. The appearance of Mo^{4+} indicates the electron injection from Cu atoms into the MoO$_3$ nanosheet, increasing the intrinsic conductivity of MoO$_3$ material [30–32]. Moreover, the O 1s spectrum is shown in Figure 4c, the peak located at 531.0 eV corresponds to the metal-oxygen bond, while the peak at 532.3 eV is ascribed to the adsorbed water [15]. In Figure 4d, the Cu 2p spectrum of the Cu-MoO$_3$ nanosheet shows the two typical peaks of 932.7 eV and 952.6 eV, which is consistent with the low valence state of Cu species [33]. The detailed oxidation state of Cu species can be analyzed by using Cu LMM. As shown in Figure S5, one typical peak located at 570.2 eV can be ascribed to the oxidation peak of Cu^{1+}. The above results confirm the successful introduction of Cu species into the MoO$_3$ nanosheet, which provides an ideal platform to study the catalytic performance of this kind of hybrid electrocatalyst.
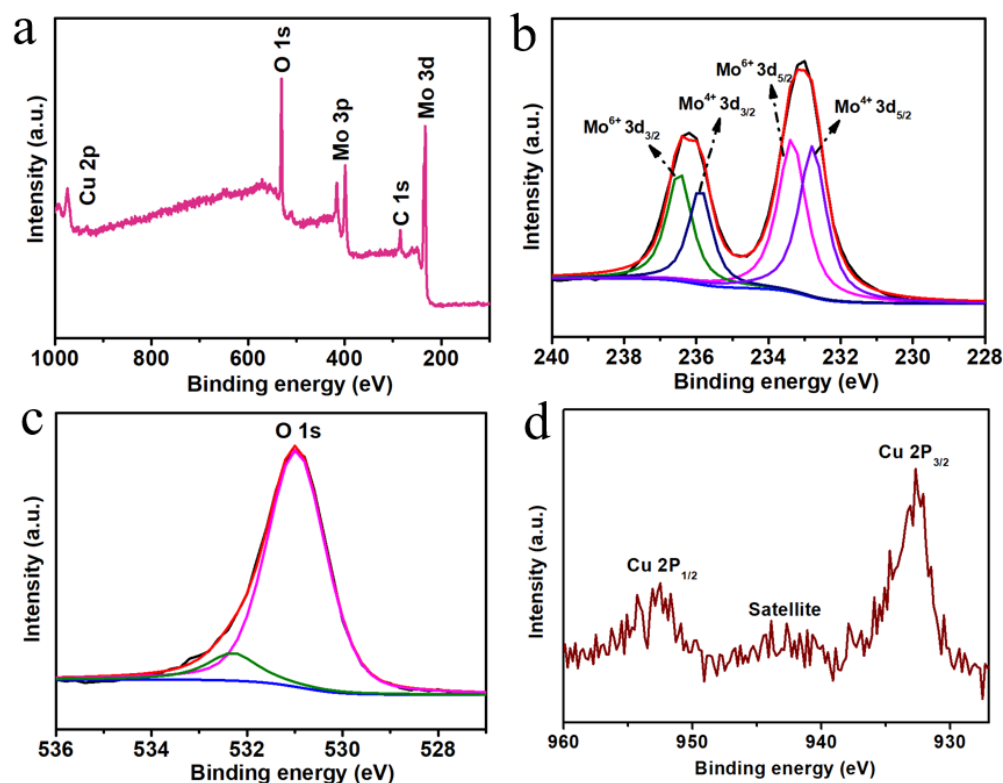

Figure 4. (**a**) XPS survey and high-resolution spectra of (**b**) Mo 3d, (**c**) O 1s and (**d**) Cu 2p of Cu doped MoO$_3$ nanosheet.

The electrocatalytic performance of obtained samples and commercial Cu foam are evaluated in 1 M KOH solution. As shown in Figure 5a, the polarization curve of commercial Cu foam exhibits poor HER performance. The current density is only 2.6 mA cm^{-2} at the overpotential of 200 mV. The improvement of catalytic activity is observed after the deposition of the MoO$_3$ sample. The MoO$_3$ catalyst exhibits an overpotential of 200 mV at 10 mA cm^{-2}, which is better than Cu foam. After the further introduction of Cu species, the HER catalytic activity realized greatly improved. The overpotential only needs 106 mV

to reach the geometric current density of 10 mA cm^{-2}, suggesting the promotion role of Cu doping for HER activity. Notably, the current density increases to 32 mA cm^{-2} at the overpotential of 200 mV, which is almost three and 10 times higher than that of MoO$_3$ and Cu foam.
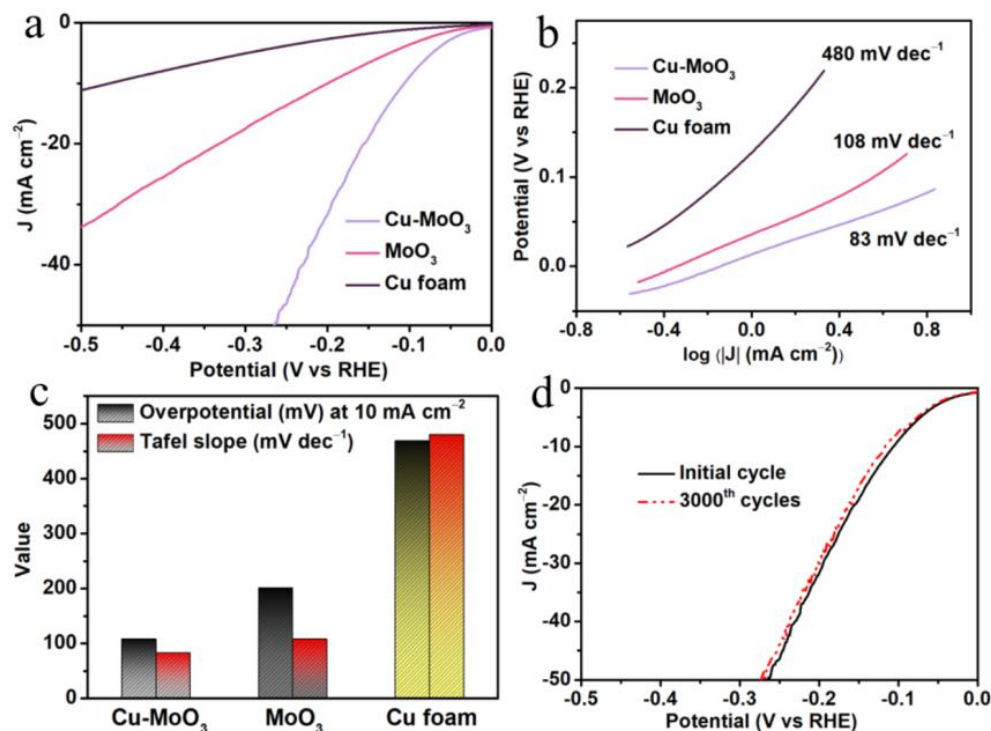

Figure 5. (**a**) The polarization curve, (**b**) Tafel slopes, (**c**) comparison of performance and (**d**) stability of as-prepared samples in 1 M KOH solution.

Moreover, the Tafel slope of those catalysts is further calculated to study the HER kinetics. As shown in Figure 5b, the obtained Cu-MoO$_3$ catalyst shows a small Tafel slope of 83 mV dec^{-1}, which is smaller than MoO$_3$ nanosheet (108 mV dec^{-1}) and Cu foam (480 mV dec^{-1}). This result indicates the Cu-MoO$_3$ catalyst possesses the faster reaction kinetics of HER to realize better catalytic activity. After systematic comparison (Figure 5c), the modification of Cu atoms induced the electron transfer, leading to the excellent catalytic activity of Cu-MoO$_3$ for HER. Stability is another important indicator to study catalysts. As shown in Figure 5d, the CV curves before and after 3000th cycling cycles confirm the similar shape of Cu-MoO$_3$, suggesting its high stability for HER in an alkaline medium. In addition, the chronoamperometric test of Cu-MoO$_3$ nanosheet delivers slight decay of current density over 100 h (Figure S4), indicating outstanding stability during a long-term HER process.

The electrochemical impedance spectroscopy (EIS) is measured to investigate the reaction kinetics of those catalysts for the HER process. As shown in Figure 6a, the curve of the Cu-MoO$_3$ nanosheet shows a smaller diameter of the semicircle (7.1 Ω) compared to the MoO$_3$ material (11.2 Ω), confirming the optimized reaction kinetics after the introduction of Mo atoms. The electrochemical surface area (ECSA) is calculated by comparing the prepared catalysts' electrochemical double layer capacitances (C$_{dl}$) with that of blank Cu foam. The fitting data are shown in Figure 6b. The Cu-MoO$_3$ nanosheet shows the highest C$_{dl}$ value of 9.8 mF cm^{-2}, which is higher than MoO$_3$ (7.3 mF cm^{-2}) and Cu foam (1.8 mF cm^{-2}). This result indicates the Cu-MoO$_3$ nanosheet has the largest surface active area, which can offer more catalytic actives during the HER process. To study the intrinsic catalytic activity, the HER performance of those samples is normalized by the C$_{dl}$ values and the results are shown in Figure 6c,d. The Cu-MoO$_3$ nanosheet still exhibits

the better catalytic performance than pristine MoO_3. This result indicates that the active specific surface area is not the only factor to improve the catalytic activity, as the electronic interaction between Cu and MoO_3 is another important factor [34–37].
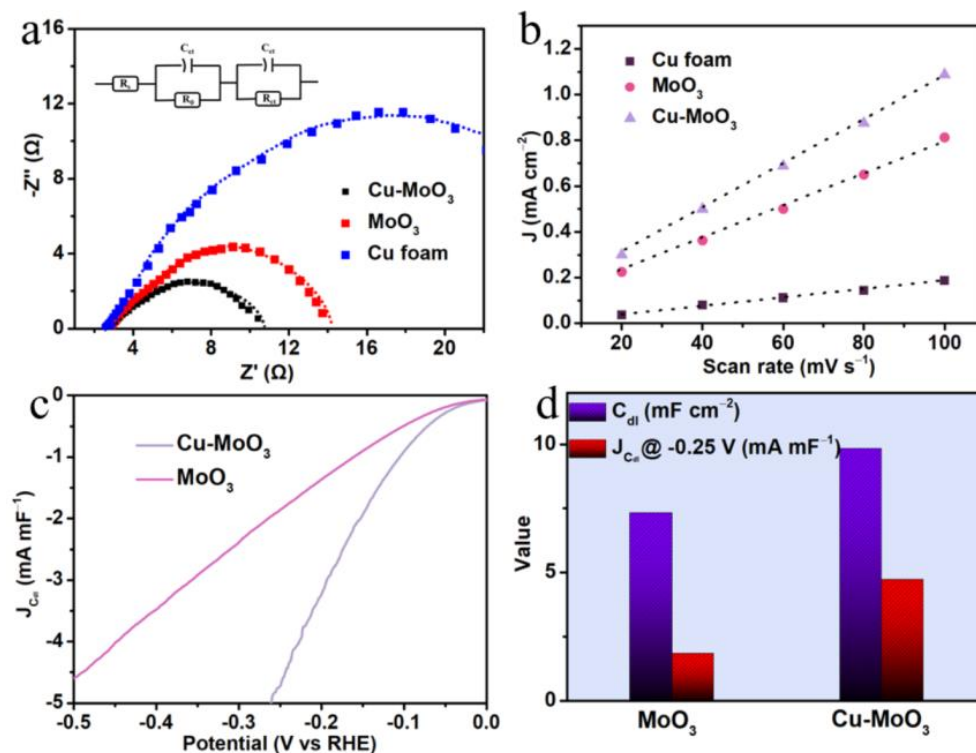

Figure 6. (**a**) The EIS spectra, inset: image of equivalent circuit model, (**b**) double-layer capacitance plots of Cu foam, MoO_3 and Cu-MoO_3, (**c**) C_{dl} normalized performance and (**d**) the performance comparison of MoO_3 and Cu-MoO_3 samples.

To analyze the effect of Cu doping on improving the HER catalytic performance, the MoO_3 nanosheet with various contents of Cu is synthesized by regulating the usage of the Cu source. As shown in Figure 7a and Figure S6, the contents of Cu are measured by the ICP method, which are 3.2%, 7.8% and 12.0% for Cu_1-MoO_3, Cu_2-MoO_3, and Cu_3-MoO_3 samples, respectively. Moreover, the HER catalytic activity of all prepared samples is tested in 1 M KOH solution. The catalytic activity increase from pristine MoO_3 sample to Cu_2-MoO_3 nanosheet, and then decrease to Cu_3-MoO_3 sample. We speculate that in Cu-doped MoO_3 electrocatalysts, the electronic conductivity and catalytically active sites are two competing relationships. When the doping amount of Cu is low, the electronic conductivity of MoO_3 material is not significantly improved, so the improvement of catalytic activity is insufficient. When the amount of Cu doping is too high, more Cu sites cover the surface of the MoO_3 catalyst to hinder the Mo catalytic active centers, resulting in a decrease in catalytic performance for HER. Therefore, those results indicate the optimal doping amount of Cu is about 7.8% in this system. In addition, the Cu_2-MoO_3 nanosheet is also used as a working electrode to analyze the Faraday efficiency of hydrogen production. As shown in Figure 7b, the Cu_2-MoO_3 nanosheet exhibits high Faraday efficiency over 97% during a long time of HER test, indicating the intrinsic high catalytic performance of Cu doped MoO_3 electrocatalyst (Figure S7).
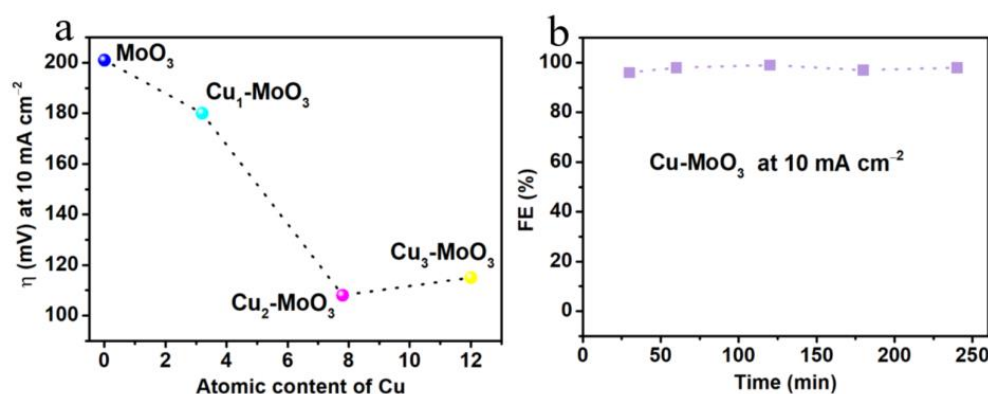
Figure 7. (a) The plots of HER catalytic performance of the MoO_3 nanosheet with different Cu doping. **(b)** The Faraday efficiency of Cu_2-MoO_3 sample at 10 mA cm^{-2} for HER.

Given the high HER catalytic activity of Cu-MoO_3 nanosheet, a simple water electrolyzer is assembled by utilizing Cu-MoO_3 and FeOOH-NF as both cathode and anode. The polarization curve of this Cu-MoO_3//FeOOH-NF water electrolyzer is shown in Figure 8a. A small voltage of 1.55 V can be realized at the current density of 10 mA cm^{-2}. In addition, the current density of the Cu-MoO_3//FeOOH-NF electrolyzer is high as 75 mA cm^{-2} at the voltage of 1.7 V. Finally, the Cu-MoO_3//FeOOH-NF electrolyzer also shows superior operation stability, which can maintain stable over 30 h at the test voltage of 1.6 V (Figure 8b). The result confirms the promising potential application of Cu-MoO_3 electrocatalyst in hydrogen generation.
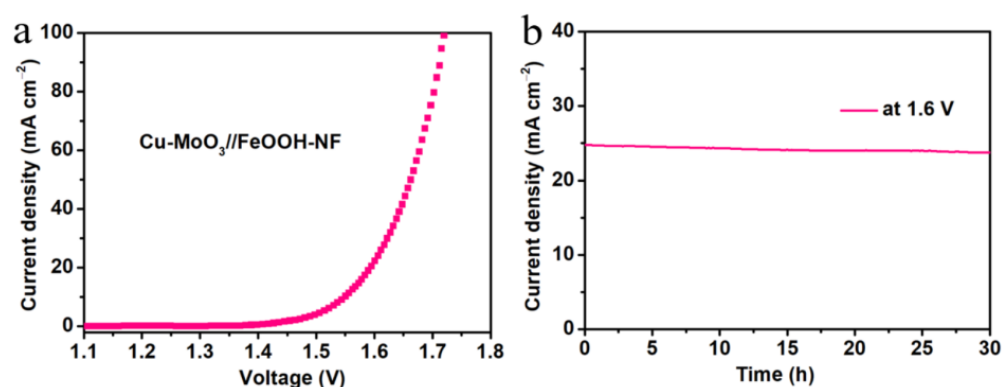

Figure 8. (a) The polarization curve of Cu-MoO_3//FeOOH-NF water electrolyzer. **(b)** The stability test of Cu-MoO_3//FeOOH-NF water electrolyzer at 1.6 V in an alkaline medium.

3. Materials and Methods

3.1. Materials

Molybdenum metal powder (Mo), hydrogen peroxide (H_2O_2), and Potassium hydroxide (KOH) are purchased from Shanghai Aladdin Biochemical Technology Co., Ltd.). Tetrakis(acetonitrile) copper(I) hexafluorophosphate is bought from Sigma. Copper foam is obtained from SaiBo electrochemical material network. All chemicals are used without any further purification.

3.2. The Synthesis of Pristine MoO_3 Nanosheet

Typically, molybdenum metal powder (2 mmol) is put into a Teflon vessel that contains 30 mL ethanol. Next, 3 mL H_2O_2 solution is added to the above solution and magnetically stirred for about 1 h. Then, a transparent yellow solution is prepared. The Teflon vessel is then sealed by a stainless steel autoclave and put into the oven at 160 °C for 12 h. After cooling to room temperature, the samples are collected by centrifugation. Next, the samples are fully rinsed with ethanol several times and dried in a vacuum oven at 80 °C.

3.3. The Synthesis of Cu-Doped MoO₃ Nanosheet

In a typical process, 30 mg MoO_3 nanosheet is first dispersed in 10 mL acetone solution by sonication treatment. Next, the uniform solution is heated to 52 °C under constant stirring. Then, different amounts of tetrakis(acetonitrile) copper(I) hexafluorophosphate are added to above solution. The reaction is kept for 20 min under stirring. The final product can be obtained by centrifugation and washed with acetone several times. The usage of Cu sources is 0.1, 0.15 and 0.2 mmol to prepare the Cu_1-MoO_3, Cu_2-MoO_3, and Cu_3-MoO_3 samples, respectively.

3.4. Structural Characterization

The X-ray diffraction (XRD) pattern is used to study the phase of prepared samples by using a Philips X'Pert Pro Super diffractometer with Cu-Kα radiation. The transmission electron microscopy (TEM) is conducted by a HT-7700 field-emission electron microscope with an acceleration voltage of 120 kV. The high-resolution TEM (HRTEM) and elemental mapping images are collected on a JEOL JEM-ARF200F TEM/STEM. The X-ray photo-electron spectroscopy (XPS) is carried out on a PHI5000 Versa Probe II XPS system. The diameter of the analyzed area is 10 μm and monochromatic X-rays are generated by an Al Kα source (1486.7 eV).

3.5. Electrochemical Measurements

A three-electrode configuration is utilized to study the electrochemical performance by using the workstation of CHI 660E. The working electrodes are obtained by drop-coating strategy. In a typical process, 5 mg samples mixed with 35 μL Nafion solution are added into 1 mL isopropyl alcohol/H_2O mixed solution and dispersed for 30 min by sonication. After the formation of a homogeneous ink, a certain volume of ink is dropped onto a clean copper foam substrate. After drying, the loading mass of catalysts is calculated to 1.5 mg cm^{-2}, and the working electrode is directly used for the electrochemical test. In addition, the 1 M KOH solution is used as an electrolyte, a saturated calomel electrode is used as the reference electrode, while the graphite rod is used as the counter electrode. The polarization curves are recorded by testing the linear sweep voltammetry (LSV) curves at 5 mV s^{-1}. The electrochemical impedance spectroscopy (EIS) is conducted at the frequency range of 100 kHz to 0.1 kHz. All presented potentials are converted to a reversible hydrogen electrode (RHE) by the Nernst equation.

4. Conclusions

In summary, a simple strategy is designed to improve the catalytic activity of MoO_3 material by the controllable modification of Cu atoms. The Cu-doped MoO_3 nanosheet is successfully prepared by hydrothermal reaction and the followed disproportionation of Cu^+. The introduction of Cu atoms not only improves the surface active area, but also transfers more electrons into the MoO_3 nanosheet, leading to more catalytic active sites and faster electron transfer ability during the HER process. As a result, the optimized Cu-MoO_3 sample shows the superior catalytic activity for HER in alkaline medium. The overpotential only needs 106 mV to reach the geometric current density of 10 mA cm^{-2}, with a small Tafel slope of 83 mV dec^{-1}. In addition, the assembled Cu-MoO_3//FeOOH-NF electrolyzer delivers the low voltage of 1.55 V at current density of 10 mA cm^{-2}. Our work opens a new way to exploit advanced low-cost electrocatalysts for large-scale hydrogen production.

prepared MoO3 nanosheet; Figure S7: The sta-bility test of Cu-MoO3 sample for HER in alkaline medium.

Author Contributions: Writing—original draft, W.H.; Writing—review and editing, P.C., and Y.T.; Validation, K.L.; methodology, D.F., Visualization, W.H.; Supervision and funding acquisition, P.C., and Y.T. This manuscript was written by the contributions of all authors. All authors have read and agreed to the published version of the manuscript.

Data Availability Statement: Data available upon request.

Conflicts of Interest: The authors declare no conflict of interest.

References

1. Xiao, X.; Yang, L.; Sun, W.; Chen, Y.; Yu, H.; Li, K.; Jia, B.; Zhang, L.; Ma, T. Electrocatalytic Water Splitting: From Harsh and Mild Conditions to Natural Seawater. *Small* **2021**, *18*, 2105830. [CrossRef]
2. Zhang, L.-N.; Li, R.; Zang, H.-Y.; Tan, H.-Q.; Kang, Z.-H.; Wang, Y.-H.; Li, Y.-G. Advanced Hydrogen Evolution Electrocatalysts Promising Sustainable Hydrogen and Chlor-Alkali Co-Production. *Energy Environ. Sci.* **2021**, *14*, 6191–6210. [CrossRef]
3. Yu, Z.-Y.; Duan, Y.; Feng, X.-Y.; Yu, X.; Gao, M.-R.; Yu, S.-H. Clean and Affordable Hydrogen Fuel from Alkaline Water Splitting: Past, Recent Progress, and Future Prospects. *Adv. Mater.* **2021**, *33*, 2007100. [CrossRef]
4. Zhang, F.; Wang, Q. Redox-Mediated Water Splitting for Decoupled H2 Production. *ACS Mater. Lett.* **2021**, *3*, 641–651. [CrossRef]
5. Kou, T.; Wang, S.; Li, Y. Perspective on High-Rate Alkaline Water Splitting. *ACS Mater. Lett.* **2021**, *3*, 224–234. [CrossRef]
6. Li, L.; Wang, P.; Shao, Q.; Huang, X. Metallic Nanostructures with Low Dimensionality for Electrochemical Water Splitting. *Chem. Soc. Rev.* **2020**, *49*, 3072–3106. [CrossRef]
7. You, B.; Sun, Y. Innovative Strategies for Electrocatalytic Water Splitting. *Acc. Chem. Res.* **2018**, *51*, 1571–1580. [CrossRef]
8. Zhao, X.; Xue, Z.; Chen, W.; Wang, Y.; Mu, T. Eutectic Synthesis of High-Entropy Metal Phosphides for Electrocatalytic Water Splitting. *ChemSusChem* **2020**, *13*, 2038–2042. [CrossRef]
9. Yang, H.; Hu, Y.; Huang, D.; Xiong, T.; Li, M.; Balogun, M.-S.; Tong, Y. Efficient Hydrogen and Oxygen Evolution Electrocatalysis by Cobalt and Phosphorus Dual-Doped Vanadium Nitride Nanowires. *Mater. Today Chem.* **2019**, *11*, 1–7. [CrossRef]
10. Wang, L.; Saveleva, V.A.; Eslamibidgoli, M.J.; Antipin, D.; Bouillet, C.; Biswas, I.; Gago, A.S.; Hosseiny, S.S.; Gazdzicki, P.; Eikerling, M.H.; et al. Deciphering the Exceptional Performance of NiFe Hydroxide for the Oxygen Evolution Reaction in an Anion Exchange Membrane Electrolyzer. *ACS Appl. Energy Mater.* **2022**, *5*, 2221–2230. [CrossRef]
11. Zhao, Y.; Sun, M.; Wen, Q.; Wang, S.; Han, S.; Huang, L.; Cheng, G.; Liu, Y.; Yu, L. Homologous NiCoP@NiFeP Heterojunction Array Achieving High-Current Hydrogen Evolution for Alkaline Anion Exchange Membrane Electrolyzers. *J. Mater. Chem. A* **2022**, *10*, 10209–10218. [CrossRef]
12. Yu, F.-Y.; Lang, Z.-L.; Yin, L.-Y.; Feng, K.; Xia, Y.-J.; Tan, H.-Q.; Zhu, H.-T.; Zhong, J.; Kang, Z.-H.; Li, Y.-G. Pt-O Bond as an Active Site Superior to Pt^0 in Hydrogen Evolution Reaction. *Nat. Commun.* **2020**, *11*, 490. [CrossRef] [PubMed]
13. Zhang, H.; Zhou, W.; Lu, X.F.; Chen, T.; Lou, X.W. (David). Implanting Isolated Ru Atoms into Edge-Rich Carbon Matrix for Efficient Electrocatalytic Hydrogen Evolution. *Adv. Energy Mater.* **2020**, *10*, 2000882. [CrossRef]
14. Pang, B.; Liu, X.; Liu, T.; Chen, T.; Shen, X.; Zhang, W.; Wang, S.; Liu, T.; Liu, D.; Ding, T.; et al. Laser-Assisted High-Performance PtRu Alloy for PH-Universal Hydrogen Evolution. *Energy Environ. Sci.* **2022**, *15*, 102–108. [CrossRef]
15. Liu, Y.; Liu, P.; Men, Y.-L.; Li, Y.; Peng, C.; Xi, S.; Pan, Y.-X. Incorporating MoO$_3$ Patches into a Ni Oxyhydroxide Nanosheet Boosts the Electrocatalytic Oxygen Evolution Reaction. *ACS Appl. Mater. Interfaces* **2021**, *13*, 26064–26073. [CrossRef]
16. Su, H.; Lou, H.; Zhao, Z.; Zhou, L.; Pang, Y.; Xie, H.; Rao, C.; Yang, D.; Qiu, X. In-Situ Mo Doped ZnIn$_2$S$_4$ Wrapped MoO$_3$ S-Scheme Heterojunction via Mo-S Bonds to Enhance Photocatalytic HER. *Chem. Eng. J.* **2022**, *430*, 132770. [CrossRef]
17. Peng, H.; Zhou, K.; Jin, Y.; Zhang, Q.; Liu, J.; Wang, H. Hierarchical Nanostructure with Ultrafine MoO$_3$ Particles-Decorated Co(OH)$_2$ Nanosheet Array on Ag Nanowires for Promoted Hydrogen Evolution Reaction. *Chem. Eng. J.* **2022**, *429*, 132477. [CrossRef]
18. Lee, D.; Kim, Y.; Kim, H.W.; Choi, M.; Park, N.; Chang, H.; Kwon, Y.; Park, J.H.; Kim, H.J. In Situ Electrochemically Synthesized Pt-MoO$_{3-x}$ Nanostructure Catalysts for Efficient Hydrogen Evolution Reaction. *J. Catal.* **2020**, *381*, 1–13. [CrossRef]
19. Duraisamy, S.; Ganguly, A.; Sharma, P.K.; Benson, J.; Davis, J.; Papakonstantinou, P. One-Step Hydrothermal Synthesis of Phase-Engineered MoS$_2$/MoO$_3$ Electrocatalysts for Hydrogen Evolution Reaction. *ACS Appl. Nano Mater.* **2021**, *4*, 2642–2656. [CrossRef]
20. Chen, P.; Tong, Y.; Wu, C.; Xie, Y. Surface/Interfacial Engineering of Inorganic Low-Dimensional Electrode Materials for Electrocatalysis. *Acc. Chem. Res.* **2018**, *51*, 2857–2866. [CrossRef]

21. Li, Y.; Yin, J.; An, L.; Lu, M.; Sun, K.; Zhao, Y.-Q.; Gao, D.; Cheng, F.; Xi, P. FeS$_2$/CoS$_2$ Interface Nanosheets as Efficient Bifunctional Electrocatalyst for Overall Water Splitting. *Small* **2018**, *14*, 1801070. [CrossRef] [PubMed]

22. Zhang, S.; Gao, G.; Zhu, H.; Cai, L.; Jiang, X.; Lu, S.; Duan, F.; Dong, W.; Chai, Y.; Du, M. In Situ Interfacial Engineering of Nickel Tungsten Carbide Janus Structures for Highly Efficient Overall Water Splitting. *Sci. Bull.* **2020**, *65*, 640–650. [CrossRef]

23. Zhang, H.; Xi, B.; Gu, Y.; Chen, W.; Xiong, S. Interface Engineering and Heterometal Doping Mo-NiS/Ni(OH)$_2$ for Overall Water Splitting. *Nano Res.* **2021**, *14*, 3466–3473. [CrossRef]

24. Ding, X.; Xia, Y.; Li, Q.; Dong, S.; Jiao, X.; Chen, D. Interface Engineering of Co(OH)$_2$/Ag/FeP Hierarchical Superstructure as Efficient and Robust Electrocatalyst for Overall Water Splitting. *ACS Appl. Mater. Interfaces* **2019**, *11*, 7936–7945. [CrossRef] [PubMed]

25. Zhang, Y.; Guo, H.; Li, X.; Du, J.; Ren, W.; Song, R. A 3D Multi-Interface Structure of Coral-like Fe-Mo-S/Ni$_3$S$_2$@NF Using for High-Efficiency and Stable Overall Water Splitting. *Chem. Eng. J.* **2021**, *404*, 126483. [CrossRef]

26. Li, L.; Zhang, T.; Yan, J.; Cai, X.; Liu, S. (Frank). P Doped MoO$_{3-x}$ Nanosheets as Efficient and Stable Electrocatalysts for Hydrogen Evolution. *Small* **2017**, *13*, 1700441. [CrossRef] [PubMed]

27. Ji, L.; Wang, J.; Teng, X.; Dong, H.; He, X.; Chen, Z. N,P-Doped Molybdenum Carbide Nanofibers for Efficient Hydrogen Production. *ACS Appl. Mater. Interfaces* **2018**, *10*, 14632–14640. [CrossRef]

28. Manikandan, A.; Ilango, P.R.; Chen, C.-W.; Wang, Y.-C.; Shih, Y.-C.; Lee, L.; Wang, Z.M.; Ko, H.; Chueh, Y.-L. A Superior Dye Adsorbent towards the Hydrogen Evolution Reaction Combining Active Sites and Phase-Engineering of (1T/2H) MoS$_2$/α-MoO$_3$ Hybrid Heterostructured Nanoflowers. *J. Mater. Chem. A* **2018**, *6*, 15320–15329. [CrossRef]

29. Kalasapurayil Kunhiraman, A.; Ramasamy, M. Nickel-Doped Nanobelt Structured Molybdenum Oxides as Electrocatalysts for Electrochemical Hydrogen Evolution Reaction. *J. Nanoparticle Res.* **2017**, *19*, 203. [CrossRef]

30. Sun, P.; Yu, H.; Liu, T.; Li, Y.; Wang, Z.; Xiao, Y.; Dong, X. Efficiently Photothermal Conversion in a MnO$_x$-Based Monolithic Photothermocatalyst for Gaseous Formaldehyde Elimination. *Chinese Chem. Lett.* **2022**, *33*, 2564–2568. [CrossRef]

31. Cheng, H.; Kamegawa, T.; Mori, K.; Yamashita, H. Surfactant-Free Nonaqueous Synthesis of Plasmonic Molybdenum Oxide Nanosheets with Enhanced Catalytic Activity for Hydrogen Generation from Ammonia Borane under Visible Light. *Angew. Chemie Int. Ed.* **2014**, *53*, 2910–2914. [CrossRef]

32. Shen, S.; Zhang, X.; Cheng, X.; Xu, Y.; Gao, S.; Zhao, H.; Zhou, X.; Huo, L. Oxygen-Vacancy-Enriched Porous α-MoO$_3$ Nanosheets for Trimethylamine Sensing. *ACS Appl. Nano Mater.* **2019**, *2*, 8016–8026. [CrossRef]

33. Koski, K.J.; Cha, J.J.; Reed, B.W.; Wessells, C.D.; Kong, D.; Cui, Y. High-Density Chemical Intercalation of Zero-Valent Copper into Bi$_2$Se$_3$ Nanoribbons. *J. Am. Chem. Soc.* **2012**, *134*, 7584–7587. [CrossRef]

34. Li, K.; Tong, Y.; Feng, D.; Chen, P. Electronic Regulation of Platinum Species on Metal Nitrides Realizes Superior Mass Activity for Hydrogen Production. *J. Colloid Interface Sci.* **2022**, *622*, 410–418. [CrossRef]

35. Li, K.; Tong, Y.; Feng, D.; Chen, P. Fluorine-Anion Engineering Endows Superior Bifunctional Activity of Nickel Sulfide/Phosphide Heterostructure for Overall Water Splitting. *J. Colloid Interface Sci.* **2022**, *625*, 576–584. [CrossRef]

36. Li, K.; Feng, D.; Tong, Y. Hierarchical Metal Sulfides Heterostructure as Superior Bifunctional Electrode for Overall Water Splitting. *ChemSusChem* **2022**, *15*, e202200590. [CrossRef]

37. Feng, D.; Zhang, S.; Tong, Y.; Dong, X. Dual-Anions Engineering of Bimetallic Oxides as Highly Active Electrocatalyst for Boosted Overall Water Splitting. *J. Colloid Interface Sci.* **2022**, *623*, 467–475. [CrossRef]